ceRNA network analysis reveals the molecular mechanism by which umbilical cord mesenchymal stem cells reverse thymic epithelial cell senescence

Zai-ling Yang
Kunming General Hospital of the People's Liberation Army: People's Liberation Army Joint Logistic Support Force 920th Hospital

Xiang-qing Zhu
Kunming General Hospital of the People's Liberation Army: People's Liberation Army Joint Logistic Support Force 920th Hospital

Tian Chuan
Kunming General Hospital of the People's Liberation Army: People's Liberation Army Joint Logistic Support Force 920th Hospital

Zhao Jing
Kunming General Hospital of the People's Liberation Army: People's Liberation Army Joint Logistic Support Force 920th Hospital

Guang-ping Ruan
Kunming General Hospital of the People's Liberation Army: People's Liberation Army Joint Logistic Support Force 920th Hospital

Pan Hang
Kunming General Hospital of the People's Liberation Army: People's Liberation Army Joint Logistic Support Force 920th Hospital

He Jie
Kunming General Hospital of the People's Liberation Army: People's Liberation Army Joint Logistic Support Force 920th Hospital

Wang Kai
Kunming General Hospital of the People's Liberation Army: People's Liberation Army Joint Logistic Support Force 920th Hospital

Wang Wei
The Affiliated Hospital of Guizhou Medical University

Xing-hua Pan (xinghuapan@aliyun.com)
Kunming General Hospital of the People's Liberation Army: People's Liberation Army Joint Logistic Support Force 920th Hospital

Research Article

Keywords: thymus senescence, thymic epithelial cell senescence, umbilical cord mesenchymal stem cells, competing endogenous RNA

Posted Date: May 11th, 2022

DOI: https://doi.org/10.21203/rs.3.rs-1595083/v1

Abstract

Background: A decreased number of thymic epithelial cells and the development of dysfunction of this population have been reported to be important factors in thymic degeneration, which can lead to thymus degeneration, proliferation defects and peripheral T-cell dysfunction. Previous research showed that umbilical cord mesenchymal stem cells can restore the structure and function of the aging thymus in vivo, but the specific mechanism is still unclear.

Methods: We treated thymic epithelial cells with H_2O_2 to establish a cellular senescence model. We assessed the effect of umbilical cord mesenchymal stem cells on thymic epithelial cells and investigated the lncRNA, miRNA and mRNA profiles of these cells. Gene Ontology and Kyoto Genome Encyclopedia analyses were performed on these RNAs to identify key pathways.

Results: Umbilical cord mesenchymal stem cells significantly reversed the H_2O_2-induced senescence of thymic epithelial cells. We identified 172 differentially expressed lncRNAs, 23 differentially expressed miRNAs and 272 differentially expressed mRNAs associated with the reversal of thymic epithelial senescence by umbilical cord mesenchymal stem cells. In addition, the PI3K-Akt signaling pathway was identified as a key signaling pathway that promotes cell proliferation by regulating the cell cycle. Finally, we constructed a lncRNA-associated competing endogenous RNA (ceRNA) network using matched miRNA, lncRNA, and mRNA expression profiles in the model dataset and altered miRNA expression profiles in umbilical cord mesenchymal stem cells.

Conclusion: Umbilical cord mesenchymal stem cells have a protective effect against H2O2-induced thymic epithelial cell senescence. Our study provides new insights into the ceRNA-mediated gene regulation of thymic senescence progression and the mechanism of action of umbilical cord mesenchymal stem cells.

Introduction

The thymus is the site where T lymphocytes develop, differentiate and mature and is an important central immune organ in the human body[1]. Paradoxically, the thymus is the first organ in the body to exhibit an age-related regression called "thymic regression"[2]. A hallmark of this early involution is a progressive decline in thymic mass and reduced output of naive T cells, leading to impaired immune function[3]. Oxidative stress has been reported as a new player in thymic degeneration and dysfunction, and the accumulation of genotoxic and proteotoxic-derived byproducts appears to adversely affect thymic tissue; conversely, enhanced antioxidant activity has been shown to improve thymus atrophy[4]. Likewise, oxidative damage is a well-documented inducer of cellular senescence, leading to cell cycle arrest, increased galactosidase activity, lipofuscin accumulation, and metabolic dysregulation[5, 6]. Considering that oxidative stress is associated with the induction of cellular senescence and thymic involution and that senescence is characterized by the accumulation of senescent cells and the decline of thymic

function, cellular senescence induced by oxidative stress may play a key role in the induction of thymic involution[7].

Thymic epithelial cells (TECs) are stromal cells that play a major role in the thymic microenvironment and in all stages of T-cell development[8]. One hypothesis regarding the cause of thymic degeneration is that aged thymic cortical and medullary TECs lack H_2O_2-metabolizing enzymes (CAT) and exhibit high ROS levels and DNA damage, causing a dramatic decrease in the number or activity of medullary TECs[9]. It has been demonstrated that CAT deficiency in TECs may make these cells more susceptible to ROS, causing early thymic atrophy[10].

Umbilical cord mesenchymal stem cells (UCMSCs) are adult stem cells derived from neonatal umbilical cord tissue, and their biological properties are similar to those of mesenchymal stem cells derived from bone marrow, adipose tissue, and dental pulp[11, 12]. There are few reports on the ability of umbilical cord mesenchymal stem cells to delay or reverse thymus aging. Jung et al. found that adipose-derived mesenchymal stem cells have a regenerative effect in a rat thymus aging model, which is manifested as an increased volume and mass of the rat thymus, and exert positive effects on the mouse thymus by promoting the proliferation of epithelial cell lines[13]. Zhan Y et al. found in a chemotherapy-induced thymus injury model that after infusion of mesenchymal stem cells, the volume of the injured thymus increased, the number of thymocytes and thymic epithelial cells increased, and the morphology of thymocytes and thymic epithelial cells recovered[14]. Our previous study showed that UCMSC treatment of aged mice inhibited thymic senescence and promoted structural and functional thymic regeneration by downregulating expression of the senescence genes p53 and p16 and upregulating expression of the SOD, Sirt1 and Sirt3 genes[15]. Thus, mesenchymal stem cells can improve the structure and function of the thymus.

Accumulating evidence suggests that noncoding RNAs (ncRNAs), such as lncRNAs and microRNAs, are involved in most pathophysiological mechanisms. miRNAs regulate gene expression by repressing posttranscriptional protein-coding (mRNAs) and noncoding genes[16, 17]. LncRNAs can exert sponge-like effects on miRNAs and mRNAs with beneficial and detrimental effects[18]. In addition, lncRNA families can also regulate molecular processes by acting as host transcripts for miRNAs[19]. There are several lines of evidence indicating that noncoding RNAs are causally related to age-related disease degeneration by regulating inflammation, cell proliferation, apoptosis, aging, and autophagy. Here, we cocultured senescent thymic epithelial cells with umbilical cord mesenchymal stem cells and assessed the changes in thymic epithelial cell proliferation, the senescent secretory phenotype, and apoptosis. To study the molecular mechanism involved, bioinformatics methods were used to comprehensively analyze the changes in the ceRNA network in TECs after coculture with UCMSCs, which provided a theoretical basis for the reversal of thymic senescence by UCMSCs.

Materials And Method

Cell source

UCMSCs were provided by the Stem Cell Bank of the Cell Biotherapy Center of the 920th Hospital of the Chinese People's Liberation Army. The proportions of surface antigens and the induction and differentiation protocols for fat, bone and cartilage were based on the literature published by our research group[20-22].

TECs were purchased from Hangzhou Meisen Biological Co., Ltd. and subcultured in culture flasks in DMEM/F12 medium containing 10% fetal bovine serum. They were then incubated at 37°C in a 5% carbon dioxide environment.

Experimental groups

Control group: Fourth-passage thymic epithelial cells were collected, the cell concentration was adjusted to 5×10^5 L-1, and 100 μL of cell suspension was inoculated into a 6-well culture plate with DMEM/F12 containing 10% fetal bovine serum for culture.

Model group: Fourth-passage thymic epithelial cells were collected, the cell concentration was adjusted to 5×10^5 L-1, and 100 μL of cell suspension was inoculated into a 6-well culture plate. When the cell fusion rate was approximately 80%, 200 μmol/L H_2O_2 (China Nanguo Pharmaceutical Co., Ltd.) was added for 72 h, and the cells were cultured in DMEM/F12 containing 10% fetal bovine serum for 48 h.

Coculture group: Fourth-passage thymic epithelial cells were collected, the cell concentration was adjusted to 5×10^5 L-1, and 100 μL of cell suspension was inoculated into 6-well culture plates. When the cell confluence rate was approximately 80%, 200 μmol/L H_2O_2 was added for 72 h. Fourth-generation umbilical cord mesenchymal stem cells were collected, the cell concentration was adjusted to 5×10^5 L-1, 100 μL of the cell suspension was inoculated into the upper Transwell chamber, and the upper Transwell chamber was placed in the 6-well plate of the model group. DMEM/F12 with 10% fetal bovine serum was used for to coculture the cells for 48 h.

Detection of the expression of Ki67, p27, CDK2 and CCNE by cellular immunofluorescence

Thymic epithelial cells from the control group, model group and coculture group were collected and fixed with paraformaldehyde. The fixative was removed by suctioning, 100 μL of membrane permeation working solution was added, the cells were incubated at room temperature for 20 min, and 3% bovine serum albumin was added to evenly cover the cells. After blocking at room temperature for 30 min, Ki67, p27, CDK2, and CCNE antibodies were added, and the samples were placed flat in a wet box and incubated overnight at 4°C. CY3/CY5/FITC goat anti-rabbit was added and incubated at room temperature for 50 min. DAPI was used to counterstain cell nuclei for 15 min, and finally, the cells were mounted with anti-fluorescence quenching mounting medium. For microscopic examination and imaging, sections were observed under a fluorescence microscope, and images were captured (DAPI emits blue light, CY3 emits red light, FITC emits green light, and CY5 emits pink light).

ELISA

The cell culture supernatant of the control, model and coculture groups was collected and centrifuged at 3000 r/min for 15 min, and the supernatant was analyzed according to the instructions provided in each ELISA kit (Human IL-6 ELISA Kit (EK106), Human IL-8 ELISA Kit (EK108) and Human VEGF ELISA Kit (EK183)).

Apoptosis assay

Thymic epithelial cells were collected from the control group, model group, and coculture group and fixed with paraformaldehyde. The fixative was removed, 100 μl of membrane permeation working solution was added, and the cells were incubated at room temperature for 20 min and washed 3 times with PBS, for 5 min each time. Buffer was then added dropwise to cover the tissue and incubated for 10 min. The appropriate amounts of TDT enzyme, dUTP, and buffer from the TUNEL kit were mixed at a ratio of 1:5:50 and incubated at 37°C for 2 hours. DAPI staining solution was added dropwise, and the samples were incubated at room temperature in the dark for 10 min. Anti-fluorescence quenching solution was used to mount coverslips on the slides with mounting medium. Microscopy and imaging: Sections were observed under a fluorescence microscope, and images were captured (DAPI emission wavelength: 420 nm, blue light; CY3 emission wavelength: 590 nm, red light).

Western blot analysis

Cells were collected from different treatment groups and lysed in RIPA buffer (Solarbio, Beijing, China). Total proteins from TECs were separated by Tris-Gly and 10% gel electrophoresis and then transferred to nitrocellulose membranes. Cell membranes were blocked with 5% skim milk for 1.5 h at room temperature, followed by incubation with primary antibodies against Bax (1:1000, ab32503), Caspase-3 (1:1000, ab32351), PI3K (1:1000, ab183957) and AKT (1:1000, GB111114) overnight. The next day, the membrane was washed with PBST and incubated with horseradish peroxidase-conjugated secondary antibody for 30 min. Protein bands were detected after treatment with SuperSignal West Femto (Thermo Fisher Science, Waltham, MA, USA). Antibodies against glyceraldehyde-3-phosphate dehydrogenase (GAPDH) and β-actin were used as internal references, and gray value analysis was performed using ImageJ software.

RNA extraction and quality control

We selected thymic epithelial cells from the control, model and coculture groups for RNA sequencing, and total RNA was extracted with TRIzol reagent (Invitrogen, Carlsbad, CA, USA). Detection of RNA quality was performed using the following methods: NanoDrop assay, Qubit 2.0 assay and Agilent 2100 Bioanalyzer assay.

Small RNA library construction

Total RNA was extracted from the sample by the TRIzol method, polyacrylamide gel (PAGE) electrophoresis was used to cut the gel to excise the band in the range of 18-30 nt, and the small RNA was recovered. The 3' linker and the 5' linker were connected, and then reverse transcription and PCR

amplification were performed on the small RNA connected to the linkers on both sides. Finally, the band of approximately 140 bp was recovered, purified by PAGE and dissolved in EBsolution to complete library construction. The constructed library was tested for quality and yield using an Agilent2100 and the ABIStepOnePlus Real-Time PCR System (Life Technologies) and sequenced on the machine. We further filtered the small RNA data obtained by preliminary filtering of the original offline data and filtered the low-quality reads from the data (the number of bases with a quality value below 20 exceeded 1 or the reads contained N). Reads with a 3' linker were intercepted before the 3' linker for later analysis; reads containing a 5' linker were filtered out; and reads containing polyA were filtered out (more than 70% of the bases in a read are A). Finally, the clean, tagged small RNA sequences were obtained for subsequent analysis.

lncRNA library construction

The eukaryotic mRNA was enriched with magnetic beads with Oligo(dT), the obtained RNA was randomly fragmented into short fragments, and the fragmented RNA was used as a template to synthesize cDNA using random hexamers. Then, buffer, dNTPs (dUTP instead of dTTP), RNase H and DNA polymerase I were added to synthesize the second strand of cDNA, which was purified by a QIAquick PCR kit, eluted with EB buffer, end repaired, and added to base A. The adaptor was sequenced, and the second strand was then degraded by the uracil-N-glycosylase (UNG) enzyme. Fragment size selection was performed by agarose gel electrophoresis, and PCR amplification was performed. The final constructed sequencing library was sequenced on an Illumina HiSeqTM 4000. The transcripts were reconstructed by stringtie; the length of the transcripts was ≥200 bp, and the number of exons was ≥2. Two software programs, CPC and CNCI, were used to predict the coding ability of new transcripts, and the intersection of these transcripts with no coding potential was taken as a reliable prediction result.

RT–qPCR verification of related genes

Quantitative PCR analysis was performed using TRIzol™ reagent, and total RNA was extracted according to the manufacturer's instructions (Invitrogen, Carlsbad, California, USA). The cDNA was amplified with reverse transcriptase (GoldenstarTMRT6. China) and Randomer primers. qPCR was performed using a CFX96TM Real-Time System (Applied 2720) according to the instructions of SYBR Green Master Mix (TsingKe Biotech Co., China). The lncRNA, mRNA, and miRNA expression levels were normalized to the expression levels of GAPDH and U6, respectively, as internal controls, and the gene expression levels were normalized by the 2-ΔΔT method. The data represent the average of three experiments, and all qPCR primers are listed in the table below.

Names	Forward primer and reverse primer
GAPDH	F: GGAGTCCACTGGCGTCTTCA
	R: GTCATGAGTCCTTCCACGATACC
U6	F: CTCGCTTCGGCAGCACA
	R: AACGCTTCACGAATTTGCGT
VEGFA	F: ATGGCAGAAGGAGGAGGG
	R: CGATTGGATGGCAGTAGC
EPHA2	F: CTCGGCTGGCTCACACAC
	R: GCTCGGGGCACTTCTTGT
MYC	F: CTGGATTTTTTTCGGGTAGTG
	R: CCTGGATGATGATGTTTTTGA
PIK3R1	F: CGAGTGGTTGGGCAATGAAA
	R: AATGCTTTACTTCGCCGTCC
BDNF	F: GTCTACCCACACGCTTCTGTATG
	R: CAGCCTTCATGCAACCAAAGTAT
ENST00000476682	F: GTTTAGGAGTGAGAGTAGCGC
	R: TGAAGAATCAGAAGAGGGTTT
ENST00000536119	F: CCTGTGCCTTCTACCTGTTCT
	R: TCCATCTGGCTCTTCTCTGTC
MSTRG.2060.1	F: TCGCTTCCTTGAATCCCTCTG
	R: TGAATCGCCTTGAACGCACAT
novel-m0297-5p	TAACTGTTTCTGCTAATTACT
hsa-miR-10399-3p	CTCTCGGACAAGCTGTAGGTC
hsa-miR-365b-5p	AGGGACTTTCAGGGGCAGCTGT
hsa-miR-3074-3p	GATATCAGCTCAGTAGGCACCG

Gene Ontology (GO) and Kyoto Encyclopedia of Genes and Genomics (KEGG) pathway analysis

Transcriptional changes at the global level were identified by GO and KEGG pathway enrichment analyses of mRNAs, miRNA target genes, and lncRNA target genes associated with UCMSC treatment. Both analyses were performed using metascape analysis.

Construction of the lncRNA-related ceRNA network

The lncRNA-related ceRNA network was established in three steps. First, we screened for targeting relationships between miRNAs and candidate ceRNAs and negative correlations between their expression levels. Second, we screened for positive correlations between the expression levels of candidate ceRNAs. Finally, candidate ceRNA binding was assessed on the basis of the degree of enrichment of the same miRNA. A lncRNA-miRNA–mRNA network was constructed using Cytoscape v3.01 software.

Statistical analysis

SPSS version 22.0 (IBM Corporation, Armonk, NY, USA) software was used for statistical analysis in our study. A p value < 0.05 indicates a statistically significant difference.

Result

UCMSCs reverse H_2O_2-induced TEC senescence

Cell proliferation activity was detected by the Ki67 cellular immunofluorescence method. Compared with the control group, the cell proliferation activity of the model group was significantly decreased, indicating that H_2O_2 inhibited the proliferation of TECs ($p<0.01$). The coculture of UCMSCs significantly increased the proliferation activity of TECs ($p<0.01$) (Fig. 1a). The SASP effect of UCMSCs on H_2O_2-treated TECs was detected. As shown in the figure, the levels of the proinflammatory factors IL-6 (Fig. 1b) and IL-8 (Fig. 1c) in the model group were higher than those in the control group and were increased after coculture with UCMSCs. The expression level of VEGF (Figure 1d) in the model group decreased, and the expression level increased after coculture with UCMSCs. The above results indicated that the SASP of senescent cells significantly changed after coculture with UCMSCs.

Figure 1: UCMSCs reverse H_2O_2-induced TEC senescence. (a) Effect of UCMSCs on H_2O_2-induced TEC cell proliferation viability (n = 3, n is the number of cells analyzed, ****P<0.0001 compared with the control group, ****P<0.0001 compared with the model group). (b-d) Statistical analysis of SASP secretion levels of senescent TECs in the presence of UCMSCs (n = 3, n is the number of cells analyzed, ***P<0.001 **P<0.01, *P<0.05).

UCMSCs attenuate H_2O_2-induced apoptosis in TECs

To study the effect of UCMSCs on H_2O_2-induced TEC apoptosis, TUNEL staining was used to detect cell apoptosis. As shown in (Fig. 2a), compared with that in the control group, the proportion of red fluorescent cells in the model group increased, indicating that after H_2O_2 induction, apoptosis was

significantly increased. After coculture with UCMSCs, apoptosis was significantly alleviated. Western blotting was used to detect the expression of the apoptosis-related proteins Bax and caspase-3. As shown in (Fig. 2b), compared with the control treatment, H_2O_2 induced a significant increase in the expression of Bax and caspase-3. After coculture with UCMSCs, the expression levels of Bax and caspase-3 were significantly reduced. This indicated that UCMSC coculture had an obvious protective effect against H_2O_2-induced apoptosis in TECs.

Figure 2: Protective effect of UCMSCs against H_2O_2-induced TEC apoptosis. (a) The effect of UCMSCs on H_2O_2-induced apoptosis was detected by TUNEL staining (n = 3, n is the number of cells analyzed; ***P< 0.001 vs. the control group, ***P<0.001 vs. the model group). (b) western blot analysis of the apoptosis-related proteins Bax and caspase-3 (n = 3, n is the number of cells analyzed; ****P<0.0001, ***P<0.001, **P<0.01).

Functional enrichment analysis of differentially expressed mRNAs

We first focused on changes in the transcript levels of coding genes using p<0.05 and |log2FC|>1.2. The volcano plot shows that 2772 differential mRNAs (1187 downregulated and 1585 upregulated) were detected between the model group and the control group. In the model group, 2260 differential mRNAs (1090 downregulated and 1170 upregulated) were detected between the groups before and after coculture (Fig. 3a and b). Using the unsupervised clustering method, the expression profiles of the top 20 up- and downregulated differentially expressed mRNAs were obtained (Fig. 3c and d). Furthermore, by comparing the gene expression of the three groups, we determined that 156 mRNAs were downregulated in the model group compared to the control group, and UCMSC coculture reversed these H_2O_2-induced mRNA changes, resulting in expression levels similar to those observed in the control group. Compared with the control group, the model group exhibited upregulation of 116 mRNAs, and these changes were also reversed after UCMSC treatment. Collectively, these results suggest that H_2O_2 induced transcriptomic alterations in TECs, which were largely reversed by UCMSC treatment (Fig. 3e).

Figure 3: Differential expression analysis of mRNAs. (a) Volcano plot of the differential mRNA expression profiles of the control group and model group. (b) Volcano plot of the differential mRNA expression profiles of the model group and coculture group. Unsupervised cluster analysis showed (c) the expression profiles of the top 20 up- and downregulated mRNAs between the control and model groups and (d) the expression profiles of the model and coculture groups. (e) Heatmap showing that 272 mRNAs showed altered expression when TECs were treated with H_2O_2; treatment with UCMSCs reversed these changes.

GO and KEGG analyses of these genes were performed to study the functions of UCMSC-targeted mRNAs, as shown in (Fig.3f). The most enriched biological processes (BPs) in the GO terms were growth, regulation of epithelial cell proliferation, and cell aging. The most enriched cellular component (CC) terms were focal adhesion, lysosome, mitochondrial membrane, etc. TThe most enriched molecular function (MF) terms were transcription factor binding, RNA polymerase II-specific DNA-binding transcription factor

binding, growth factor binding, etc. The top enriched KEGG pathways are shown in (Fig.3g). The MAPK signaling pathway, cAMP signaling pathway, VEGF signaling pathway, PI3K-Akt signaling pathway, apoptosis, etc., may be related to the reversal of TEC senescence by UCMSCs.

Figure 3: Functional enrichment analysis of differentially expressed mRNAs (f) and GO enrichment analysis of UCMSC-altered mRNAs. The superscript numbers represent the number of genes and P values marked on the GO item, and the ordinate represents the GO item. (g) KEGG enrichment analysis of mRNAs with altered expression in the presence of UCMSCs. The superscript numbers indicate the number of genes and P value values marked on the GO item, and the ordinate is the KEGG pathway.

Functional enrichment analysis of differentially expressed lncRNAs

Using the same method (log2(FC)>1.2 and p<0.05), volcano plots were generated to compare the differential lncRNA expression profiles of the "model group vs. control group" and "UCMSC group vs. model group". (Fig.4a) shows that compared with the control group, the model group had 1120 differentially expressed lncRNAs (555 upregulated and 565 downregulated), and compared with the model group, UCMSCs had 1033 differentially expressed lncRNAs (558 upregulated and 475 downregulated) (Fig. 4b). Similar to mRNAs, the expression profiles of the top 20 up- and downregulated differentially expressed lncRNAs are shown in (Fig.4c and d). Compared with the control group, the model group exhibited 172 lncRNAs that were significantly abnormally expressed (67 were upregulated, and 105 were downregulated). After treatment with UCMSCs, these H_2O_2-induced lncRNA changes were reversed, resulting in expression levels similar to those in the control group. (Fig. 4e).

Figure 4: Analysis of differential expression of lncRNAs and volcano plots of the expression profiles of differentially expressed lncRNAs (a) between the control group and the model group and (b) between the model group and the UCMSC group. Unsupervised cluster analysis showed the expression profiles of the top 20 up- and downregulated lncRNAs (c) between the control and model groups and (d) between the model and coculture groups. (g) Heatmap showing 172 lncRNAs that were altered by H2O2 in TECs; treatment with UCMSCs reversed these alterations. As shown in Figure (4e),

GO analysis of UCMSC-targeted potential lncRNA target genes indicated that the most enriched GO terms included regulation of epithelial cell differentiation, morphogenesis of an epithelium, epithelial and cell differentiation (BP); focal adhesion and cell-substrate junction (CC); and growth factor activity and protein domain specific binding (MF)(Fig. 4f). As shown in (Fig. 4g), the apoptosis, cell cycle and VEGF signaling pathways were enriched in the KEGG analysis of potential lncRNA target genes.

Figure 4: Differentially expressed lncRNA functional enrichment analysis. (f) GO enrichment analysis of UCMSC-altered lncRNA target genes. The superscript numbers represent the number of genes and P values marked on the GO item, and the ordinate represents the GO item. (g) KEGG enrichment analysis of UCMSC-altered lncRNAs. The superscript numbers indicate the number of genes and P values marked on the GO item, and the ordinate is the KEGG pathway.

Functional enrichment analysis of differentially expressed miRNAs

After comparing the miRNA transcriptomes of different groups, volcano plot (Fig. 5a and b) analysis revealed 208 H_2O_2-responsive miRNAs (i.e., 100 upregulated and 108 downregulated in the H_2O_2 intervention group) and 175 UCMSC-responsive miRNAs (i.e., 102 were upregulated and 73 were downregulated after UCMSC treatment). The results of unsupervised clustering analysis revealed that the top 20 differentially expressed miRNAs were upregulated and downregulated (Fig. 5c and d). Compared with the control group, the model group exhibited downregulated expression of 12 miRNAs, and this effect was reversed after UCMSC treatment. Compared with the control treatment, the H_2O_2 intervention induced upregulation of 11 miRNAs, and after coculture with UCMSCs, the levels of these miRNAs were similar to those in the control group (Fig. 5e).

Figure 5: Differential expression analysis of miRNAs and volcano plots of DE miRNA expression profiles (a) between the control and model groups and (b) between the model and coculture groups. Unsupervised cluster analysis showed the expression profiles of the top 20 miRNAs that were up- and downregulated between the control and model groups. (c) and (d) The expression profiles of the model and coculture groups. (e) Heatmap showing 23 miRNAs that were altered when TECs were subjected to H_2O_2-induced senescence, which was reversed by UCMSCs.

In the GO analysis (Fig. 5f), the BP terms were cell differentiation, growth and apoptotic process. MFs were mainly enriched in RNA polymerase II regulatory region sequence-specific DNA binding and growth factor receptor binding. Regarding CCs, the enriched terms included chromatin, mitochondrial outer membrane, and lysosome. The most enriched KEGG pathways are shown in (Fig. 5g). Major genes were enriched in the following pathways: FoxO signaling pathway, EGFR tyrosine kinase inhibitor resistance, MAPK signaling pathway, Jak-STAT signaling pathway, etc. These results suggest that miRNA-regulated target mRNAs may participate in the protective function of UCMSCs through these pathways. The PI3K-AKT signaling pathway has also been found to be closely related to this process.

Figure 5: Functional enrichment analysis of differentially expressed miRNAs. (f) GO enrichment analysis of target genes of miRNAs altered by UCMSCs. The superscript numbers represent the number of genes and P values marked on the GO item, and the ordinate represents the GO item. (g) KEGG enrichment analysis of UCMSC-altered lncRNAs. The superscript numbers indicate the number of genes and P values marked on the GO item, and the ordinate is the KEGG pathway.

RT–qPCR verification of related genes

We performed RT–qPCR analysis to validate the results of RNA-seq. Among the differentially expressed mRNAs most strongly associated with the reversal of TEC senescence by UCMSCs, we selected 5 mRNAs enriched in the PI3K-AKT signaling pathway for real-time qPCR: VEGFA, EPHA2, BDNF, MYC, and PIK3R1. In addition, abnormally regulated noncoding RNAs were selected for real-time qPCR analysis, with 5 miRNAs (novel-m0297-5p, hsa-miR-10399-3p, hsa-miR-365b-5p, hsa-miR-3074-3p, hsa-miR-3691-5p) and 3 lncRNAs (ENST00000476682, ENST00000536119, MSTRG.2060.1). As shown in Figure (6), the

expression levels detected by RT–qPCR were consistent with the results of RNA-Seq. Therefore, all of these lncRNAs, miRNAs and mRNAs were identified as targets closely related to UCMSC therapy and included in subsequent analyses.

Figure 6: RT–qPCR-validated differential expression of ncRNAs and mRNAs. The data show that the expression levels of lncRNAs (ENST00000476682, ENST00000536119, MSTRG.2060.1), microRNAs (novel-m0297-5p, hsa-miR-10399-3p, hsa-miR-365b-5p, hsa-miR-3074-3p, hsa- miR-3691-5p), and mRNAs (VEGFA, EPHA2, BDNF, MYC, PIK3R1) and the RT–qPCR results were consistent with the RNA sequencing results.

UCMSCs activate the PI3K-AKT pathway in H_2O_2-injured TECs to regulate the TEC cell cycle

Combined with the results of KEGG analysis, we speculated that the PI3K-AKT pathway may be the key pathway by which UCMSCs reverse TEC senescence. As shown in (Fig. 7a), compared with those in the model group, the levels of the PI3K and AKT proteins in the UCMSC group increased, suggesting that PI3K and AKT protein levels were elevated under the action of UCMSCs. At the same time, we detected the expression of p27 (Fig. 7b), CDK2 (Fig. 7c) and CCNE (Fig. 7D), the key nodes that regulate the cell cycle downstream of PI3K. The expression of p27 decreased and the expression of CDK2 and CCNE increased after coculture. This result indicates that UCMSCs may induce senescent TECs to enter the proliferation and replication phase by activating the PI3K-AKT signaling pathway.

Figure 7: UCMSCs activate the PI3K-AKT pathway in senescent TECs. (a) The expression of PI3K-AKT signaling pathway proteins was detected by western blotting, and GAPDH was used as a control. (b-d) Immunofluorescence detection of the expression of p27, CDK2 and CCNE at key sites of cell cycle regulation downstream of the PI3K signaling pathway.

A comprehensive network analysis of lncRNA-associated ceRNAs

In this study, Miranda (v3.3a) and TargetScan (Version: 7.0) software was used to perform target gene prediction, and the intersection of the target gene prediction results obtained with the two software programs was used as the result of miRNA target gene prediction. Based on the identified differentially expressed RNAs between the control and model groups, a lncRNA-related ceRNA network (containing 19 mRNAs, 33 lncRNAs, and 6 miRNAs) associated with H_2O_2-induced TEC senescence was constructed (Fig. 8). Furthermore, treatment with UCMSCs affected the expression of 14 lncRNAs, which subsequently regulated 11 mRNAs by competitively binding to 3 miRNAs (miR-93-x, miR-181-x, and novel-0297-5p). The arrows inside the lncRNA-miRNA–mRNA network represent the changes in RNA levels after coculture with UCMSCs. Overall, evidence from our bioinformatics analysis suggests that lncRNAs contain miRNA-responsive elements and play key regulatory roles.

Figure 8: LncRNA-miRNA–mRNA interaction network. Circles represent mRNAs, squares represent lncRNAs, and triangles represent miRNAs. Red and green represent up- and downregulation in the model group, respectively. Arrows indicate UCMSC-altered RNAs, and downward arrows indicate downregulation.

Discussion

To our knowledge, this is the first comprehensive study of the lncRNA-associated ceRNA network, revealing that UCMSCs enable senescent TECs to reverse their senescence through the ceRNA molecular network. Our results showed that compared with H_2O_2 treatment, UCMSC coculture significantly increased cell proliferation and inhibited apoptosis. In addition, 172 differentially expressed lncRNAs, 23 differentially expressed miRNAs, and 272 differentially expressed mRNA associations were identified, and the sequencing results were verified by RT–qPCR. Evidence from KEGG enrichment functional analysis indicated that UCMSCs reversed TEC senescence, possibly via regulation of the cell cycle by the PI3K/AKT signaling pathway, which was further confirmed by western blotting and cellular immunofluorescence. Based on authoritative databases, the lncRNA-associated ceRNA network was visualized, and miRNAs, lncRNAs and mRNAs were comprehensively analyzed. This approach may provide new ideas for the treatment of thymic aging.

First, we focused on differentially expressed encoded genes. A total of 2772 genes with H_2O_2-induced changes were detected, of which 1585 genes were upregulated and 1187 genes were downregulated. In addition, a total of 2260 UCMSC-induced altered genes were identified (1090 upregulated, 1170 downregulated). By comparing the gene expression data of the three groups, we ultimately identified 272 mRNAs that may be involved in the protective effect of UCMSCs against H_2O_2-induced TEC senescence. Among other genes that have been previously annotated, some are involved in the mechanisms of oxidative stress. DDIT4 has been shown to inhibit mTOR and the cyclin-dependent kinase inhibitor p21 and protect cells from stress-induced premature senescence[23, 24]. Sestrin2 (SESN2) is a good regulator of autophagy and the antioxidant response responsible for reducing the accumulation of ROS and inhibiting mTORC1 signaling, a new target for antiaging research[25, 26]. HCAR3 and HCAR2 are G protein-coupled receptors that activate downstream targets at the PI3K/Akt signaling level to control cell proliferation and survival in a cell-type-specific manner[27, 28]. VEGFA is a family of growth factors that regulate cell proliferation during aging[29, 30]. Compared with the control group, the expression levels of DDIT4, SESN2, HCAR3, HCAR2, PTGS2, and VEGFA were decreased in the H_2O_2-treated group, and interestingly, the expression of these genes was upregulated to normal levels after coculture with UCMSCs; these mRNAs are important in thymic aging-related diseases. The specific factors associated with the senescence-reversing effect of UCMSCs deserve further investigation.

LncRNAs have negative or positive effects on oxidative stress-induced aging[31, 32]. Therefore, studying lncRNAs involved in thymic epithelial cell senescence may contribute to further research on specific biomarkers of thymic senescence-related diseases. In our study, a total of 1120 lncRNAs were found to be associated with H_2O_2-induced TEC senescence, and a large number of lncRNAs were functionally described. In addition, a total of 277 lncRNAs were found to play a role in the reversal of TEC senescence by UCMSCs. However, knowledge concerning the potential functions of these lncRNAs is limited, and future studies should determine the exact mechanisms of lncRNAs in the reversal of TEC senescence by UCMSCs.

Oxidative stress is an upstream regulator or downstream effector of miRNAs involved in the regulation of thymic aging in mice[33, 34]. However, its regulatory mechanism still needs extensive research. In this study, a total of 208 miRNAs were observed to cause changes during H_2O_2 treatment, and a few miRNAs were found to play an important role in the reversal of thymic epithelial aging by UCMSCs. Interestingly, these aging-related miRNAs were all newly discovered. Further studies are needed to reveal the functions of these miRNAs in the aging process of the thymus and their specific roles in the mechanism of UCMSC treatment.

The potential functions of the differential mRNAs and lncRNAs identified in this study were further predicted by KEGG pathway analysis. Pathway analysis of mRNA indicated that the PI3K signaling pathway plays an important role in the reversal of thymic epithelial cell senescence by UCMSCs. Western blotting results showed that the levels of PI3K and AKT increased during the reversal of senescence in UCMSCs, resulting in a decrease in the expression of p27, a key node that regulates the cell cycle downstream of AKT, and an increase in the expression of CDK2 and CCNE by reducing the inhibition of CDK2 and CCNE, indicating that UCMSCs regulate PI3K/AKT. The p27 signaling pathway regulates the thymic epithelial cell cycle. As previously mentioned, the PI3K/Akt pathway is important for the regulation of cell cycle progression[35, 36], is involved in the alteration of p27 activity, and subsequently abolishes its inhibition of the Cdk2/cyclin A and Cdk2/cyclin E complexes, enhances the kinase activity of cells from late G1 to S phase, and promotes cell replication and proliferation[37, 38].

RNA transcripts and lncRNAs with miRNA-responsive elements may act as ceRNAs to repress miRNA function through mutual regulation by shared miRNA-responsive elements[39]. In this study, we constructed a putative lncRNA-miRNA–mRNA network describing the mechanism by which lncRNAs act as ceRNAs. This mechanism may regulate mRNA expression by regulating the levels of its upstream miRNA regulators. We identified certain lncRNAs that act as sponges to participate in the protective effect of UCMSCs against TEC senescence. The results showed that 14 UCMSC-targeted lncRNAs could competitively bind to miR-93-x, miR-181-x, and novel-0297-5p, thereby regulating the expression of 11 mRNAs. Notably, additional studies are needed to further elucidate this coexpression network.

In conclusion, the coding and noncoding transcriptomes of TECs were altered in the control, model and coculture groups. Considering the above results and bioinformatics analysis results, this study showed that abnormally expressed miRNAs, lncRNAs and mRNAs were involved in several specific biological processes and were involved in pathways related to H_2O_2-induced TEC senescence and UCMSC reversal of senescence. To more accurately elucidate the mechanism of reversal of TEC senescence by UCMSCs, future studies need to overcome several limitations. Changes in ncRNAs and mRNAs in other senescent cells and animal models should also be observed. In addition, further validation studies are needed to determine the key factors regulating thymic epithelial cell senescence.

Conclusion

i The proliferation ability of aging thymic epithelial cells was weakened, the expression of the proinflammatory factors IL-6 and IL-8 was increased, and the expression of VEGF was decreased.

ii The number of apoptotic cells increased in aging thymic epithelial cells, and the expression of the apoptosis-related proteins Bax and caspase-3 increased. After coculture, the number of apoptotic cells decreased, and the expression of apoptosis-related proteins decreased.

iii We established a network of ceRNAs related to the reversal of TEC senescence by UCMSCs and identified the phosphatidylinositol-3-kinase/protein kinase B pathway as a key signaling pathway involved in regulating the cell cycle.

Abbreviations

UCMSCs: Umbilical cord mesenchymal stem cells;TEC: Thymus epithelial cells;ceRNA: Competing endogenous RNA;CDK2: CDKN2;miRNA: microRNA;P27: cyclin-dependent kinase inhibitor 1B;CCNE: cyclin E;BAX: BCL2 associated X;VEGF: vascular endothelial growth factor;

Declarations

Ethics approval and consent to participate

All experimental protocols were approved by the relevant committees of the 920th Hospital of the Joint Logistics Support Force of the Chinese People's Liberation Army and the approval number was Lengshen 2021-017 (Section)-01

Consent for publication

Not applicable.

Availability of data and materials

All data generated or analyzed during this study are included in this published article.

Competing interests

The authors declare that they have no competing interests.

Funding

This work was supported by grants from the Yunnan Science and Technology Plan Project Major Science and Technology Project (2018ZF007) and the project entitled “Transformation of subtotipotent stem cells based on the tree shrew model of multiple organ dysfunction syndrome” (SYDW[2020]19).

Authors’ contributions

XHP and WW designed the study. ZLY, XQZ, TC, ZJ, RGP ,PH performed the experiments and collected the data. ZLY wrote the manuscript. HJ, WK assisted with the literature searches and revised the manuscript. All authors read and approved the final manuscript.

Acknowledgments

We thank everyone on our team for assisting with the preparation of this manuscript.

Author details

1. The Basic Medical Laboratory of the 920th Hospital of Joint Logistics Support Force of PLA, The Transfer Medicine Key Laboratory of Cell Therapy Technology of

Yunan Province, The Integrated Engineering Laboratory of Cell Biological Medicine

of State and Regions, Kunming 650032, Yunnan Province, China.

2.Affiliated Tumor Hospital of Guizhou Medical University,Medical laboratory, Guiyang 55000, Guizhou Province, China.

References

1. Baran-Gale J, Morgan MD, Maio S, Dhalla F, Calvo-Asensio I, Deadman ME, et al. Ageing compromises mouse thymus function and remodels epithelial cell differentiation. Elife. 2020;9.
2. Taub DD, Longo DL. Insights into thymic aging and regeneration. Immunol Rev. 2005;205:72-93.
3. Gui J, Mustachio LM, Su DM, Craig RW. Thymus Size and Age-related Thymic Involution: Early Programming, Sexual Dimorphism, Progenitors and Stroma. Aging Dis. 2012;3:280-90.
4. Griffith AV, Venables T, Shi J, Farr A, van Remmen H, Szweda L, et al. Metabolic Damage and Premature Thymus Aging Caused by Stromal Catalase Deficiency. Cell Rep. 2015;12:1071-9.
5. Gorgoulis V, Adams PD, Alimonti A, Bennett DC, Bischof O, Bishop C, et al. Cellular Senescence: Defining a Path Forward. Cell. 2019;179:813-27.
6. Salama R, Sadaie M, Hoare M, Narita M. Cellular senescence and its effector programs. Genes Dev. 2014;28:99-114.
7. Barbouti A, Vasileiou P, Evangelou K, Vlasis KG, Papoudou-Bai A, Gorgoulis VG, et al. Implications of Oxidative Stress and Cellular Senescence in Age-Related Thymus Involution. Oxid Med Cell Longev. 2020;2020:7986071.
8. Xing Y, Jameson SC, Hogquist KA. Thymoproteasome subunit-beta5T generates peptide-MHC complexes specialized for positive selection. Proc Natl Acad Sci U S A. 2013;110:6979-84.
9. Hamazaki Y, Sekai M, Minato N. Medullary thymic epithelial stem cells: role in thymic epithelial cell maintenance and thymic involution. Immunol Rev. 2016;271:38-55.

10. Barbouti A, Evangelou K, Pateras IS, Papoudou-Bai A, Patereli A, Stefanaki K, et al. In situ evidence of cellular senescence in Thymic Epithelial Cells (TECs) during human thymic involution. Mech Ageing Dev. 2019;177:88-90.
11. Liu Y, Li C, Wang S, Guo J, Guo J, Fu J, et al. Human umbilical cord mesenchymal stem cells confer potent immunosuppressive effects in Sjogren's syndrome by inducing regulatory T cells. Mod Rheumatol. 2021;31:186-96.
12. Baharlooi H, Nouraei Z, Azimi M, Moghadasi AN, Tavassolifar MJ, Moradi B, et al. Umbilical cord mesenchymal stem cells as well as their released exosomes suppress proliferation of activated PBMCs in multiple sclerosis. Scand J Immunol. 2021;93:e13013.
13. Jung WS, Han SM, Kim SM, Kim ME, Lee JS, Seo KW, et al. Stimulatory effect of HGF-overexpressing adipose tissue-derived mesenchymal stem cells on thymus regeneration in a rat thymus involution model. Cell Biol Int. 2014;38:1106-17.
14. Zhan Y, Wang L, Liu G, Zhang X, Yang J, Pan Y, et al. The Reparative Effects of Human Adipose-Derived Mesenchymal Stem Cells in the Chemotherapy-Damaged Thymus. Stem Cells Dev. 2019;28:186-95.
15. Pan XH, Lin QK, Yao X, Li ZA, Cai XM, Pang RQ, et al. Umbilical cord mesenchymal stem cells protect thymus structure and function in aged C57 mice by downregulating aging-related genes and upregulating autophagy- and anti-oxidative stress-related genes. Aging (Albany NY). 2020;12:16899-920.
16. Greco S, Gorospe M, Martelli F. Noncoding RNA in age-related cardiovascular diseases. J Mol Cell Cardiol. 2015;83:142-55.
17. Fabian MR, Sonenberg N, Filipowicz W. Regulation of mRNA translation and stability by microRNAs. Annu Rev Biochem. 2010;79:351-79.
18. Kartha RV, Subramanian S. Competing endogenous RNAs (ceRNAs): new entrants to the intricacies of gene regulation. Front Genet. 2014;5:8.
19. Shi Y, Liu JB, Deng J, Zou DZ, Wu JJ, Cao YH, et al. The role of ceRNA-mediated diagnosis and therapy in hepatocellular carcinoma. Hereditas. 2021;158:44.
20. Pan XH, Zhou J, Yao X, Shu J, Liu JF, Yang JY, et al. Transplantation of induced mesenchymal stem cells for treating chronic renal insufficiency. Plos One. 2017;12:e176273.
21. Pan XH, Huang X, Ruan GP, Pang RQ, Chen Q, Wang JX, et al. Umbilical cord mesenchymal stem cells are able to undergo differentiation into functional islet-like cells in type 2 diabetic tree shrews. Mol Cell Probes. 2017;34:1-12.
22. Pan XH, Chen YH, Yang YK, Zhang XJ, Lin QK, Li ZA, et al. Relationship between senescence in macaques and bone marrow mesenchymal stem cells and the molecular mechanism. Aging (Albany NY). 2019;11:590-614.
23. Li XH, Ha CT, Fu D, Xiao M. REDD1 protects osteoblast cells from gamma radiation-induced premature senescence. Plos One. 2012;7:e36604.

24. Cho WK, Kim HI, Kim SY, Seo HH, Song J, Kim J, et al. Anti-Aging Effects of Leontopodium alpinum (Edelweiss) Callus Culture Extract Through Transcriptome Profiling. Genes (Basel). 2020;11.
25. Piochi LF, Machado IF, Palmeira CM, Rolo AP. Sestrin2 and mitochondrial quality control: Potential impact in myogenic differentiation. Ageing Res Rev. 2021;67:101309.
26. Sun W, Wang Y, Zheng Y, Quan N. The Emerging Role of Sestrin2 in Cell Metabolism, and Cardiovascular and Age-Related Diseases. Aging Dis. 2020;11:154-63.
27. Sun H, Li G, Zhang W, Zhou Q, Yu Y, Shi Y, et al. Niacin activates the PI3K/Akt cascade via PKC- and EGFR-transactivation-dependent pathways through hydroxyl-carboxylic acid receptor 2. Plos One. 2014;9:e112310.
28. Jadeja RN, Jones MA, Fromal O, Powell FL, Khurana S, Singh N, et al. Loss of GPR109A/HCAR2 induces aging-associated hepatic steatosis. Aging (Albany NY). 2019;11:386-400.
29. Gorenjak V, Petrelis AM, Stathopoulou MG, Toupance S, Kumar S, Labat C, et al. A genetic determinant of VEGF-A levels is associated with telomere attrition. Aging (Albany NY). 2021;13:23517-26.
30. Stocco E, Barbon S, Tortorella C, Macchi V, De Caro R, Porzionato A. Growth Factors in the Carotid Body-An Update. Int J Mol Sci. 2020;21.
31. Fuschi P, Carrara M, Voellenkle C, Garcia-Manteiga JM, Righini P, Maimone B, et al. Central role of the p53 pathway in the noncoding-RNA response to oxidative stress. Aging (Albany NY). 2017;9:2559-86.
32. Kim C, Kang D, Lee EK, Lee JS. Long Noncoding RNAs and RNA-Binding Proteins in Oxidative Stress, Cellular Senescence, and Age-Related Diseases. Oxid Med Cell Longev. 2017;2017:2062384.
33. Konovalova J, Gerasymchuk D, Parkkinen I, Chmielarz P, Domanskyi A. Interplay between MicroRNAs and Oxidative Stress in Neurodegenerative Diseases. Int J Mol Sci. 2019;20.
34. Ye Y, Li D, Ouyang D, Deng L, Zhang Y, Ma Y, et al. MicroRNA expression in the aging mouse thymus. Gene. 2014;547:218-25.
35. Cai B, Zheng Y, Ma S, Xing Q, Wang X, Yang B, et al. Long noncoding RNA regulates hair follicle stem cell proliferation and differentiation through PI3K/AKT signal pathway. Mol Med Rep. 2018;17:5477-83.
36. Sun W, Zhu J, Li S, Tang C, Zhao Q, Zhang J. Selenium supplementation protects against oxidative stress-induced cardiomyocyte cell cycle arrest through activation of PI3K/AKT. Metallomics. 2020;12:1965-78.
37. Guo Q, Xiong Y, Song Y, Hua K, Gao S. ARHGAP17 suppresses tumor progression and up-regulates P21 and P27 expression via inhibiting PI3K/AKT signaling pathway in cervical cancer. Gene. 2019;692:9-16.
38. Zhang K, Yang Y, Ge H, Wang J, Chen X, Lei X, et al. Artesunate promotes the proliferation of neural stem/progenitor cells and alleviates Ischemia-reperfusion Injury through PI3K/Akt/FOXO-3a/p27(kip1) signaling pathway. Aging (Albany NY). 2020;12:8029-48.
39. Lin YH. MicroRNA Networks Modulate Oxidative Stress in Cancer. Int J Mol Sci. 2019;20.

Figures

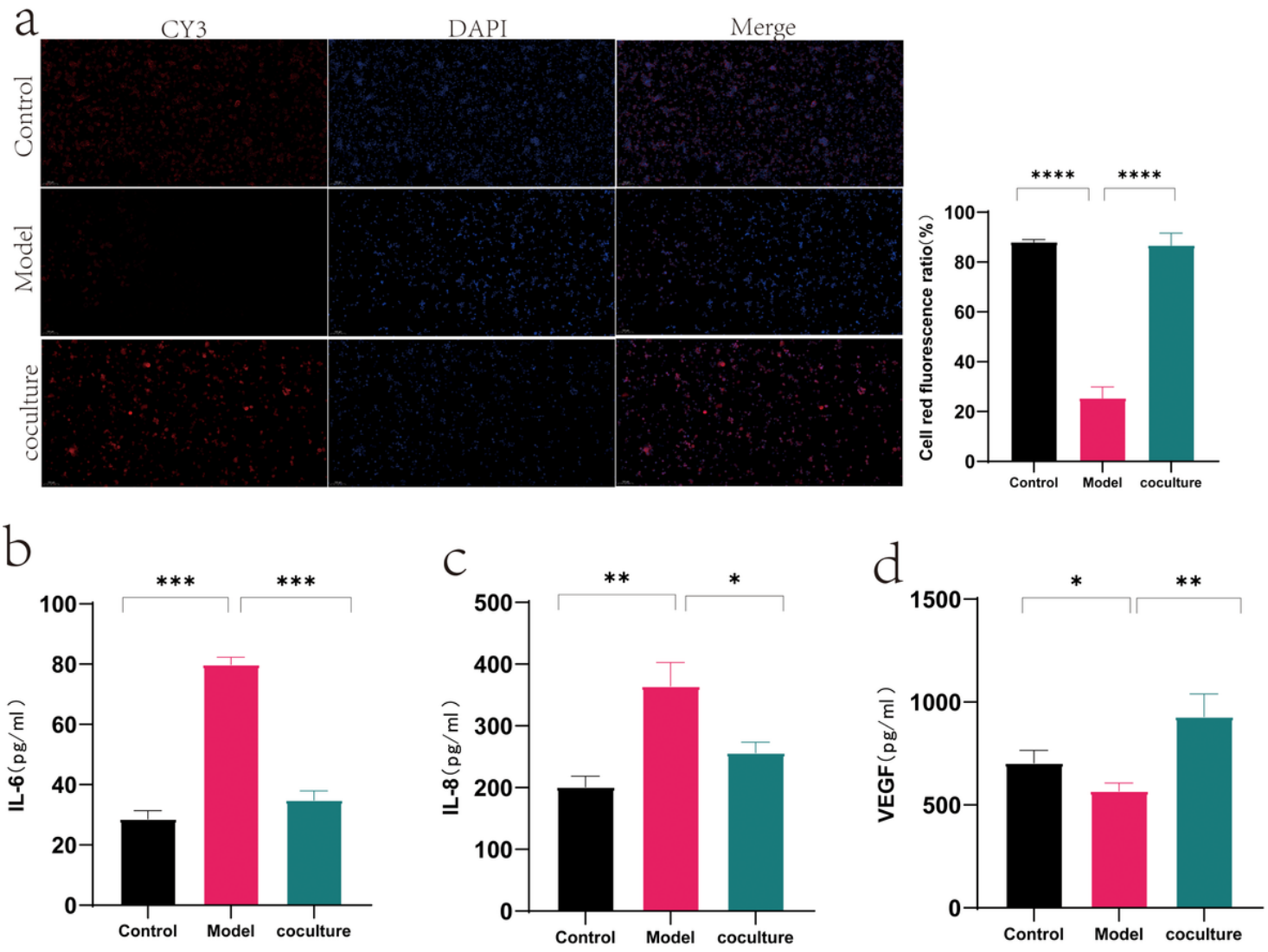

Figure 1

UCMSCs reverse H_2O_2-induced TEC senescence. (a) Effect of UCMSCs on H_2O_2-induced TEC cell proliferation viability (n = 3, n is the number of cells analyzed, ****P<0.0001 compared with the control group, ****P<0.0001 compared with the model group). (b-d) Statistical analysis of SASP secretion levels of senescent TECs in the presence of UCMSCs (n = 3, n is the number of cells analyzed, ***P<0.001 **P<0.01, *P<0.05).

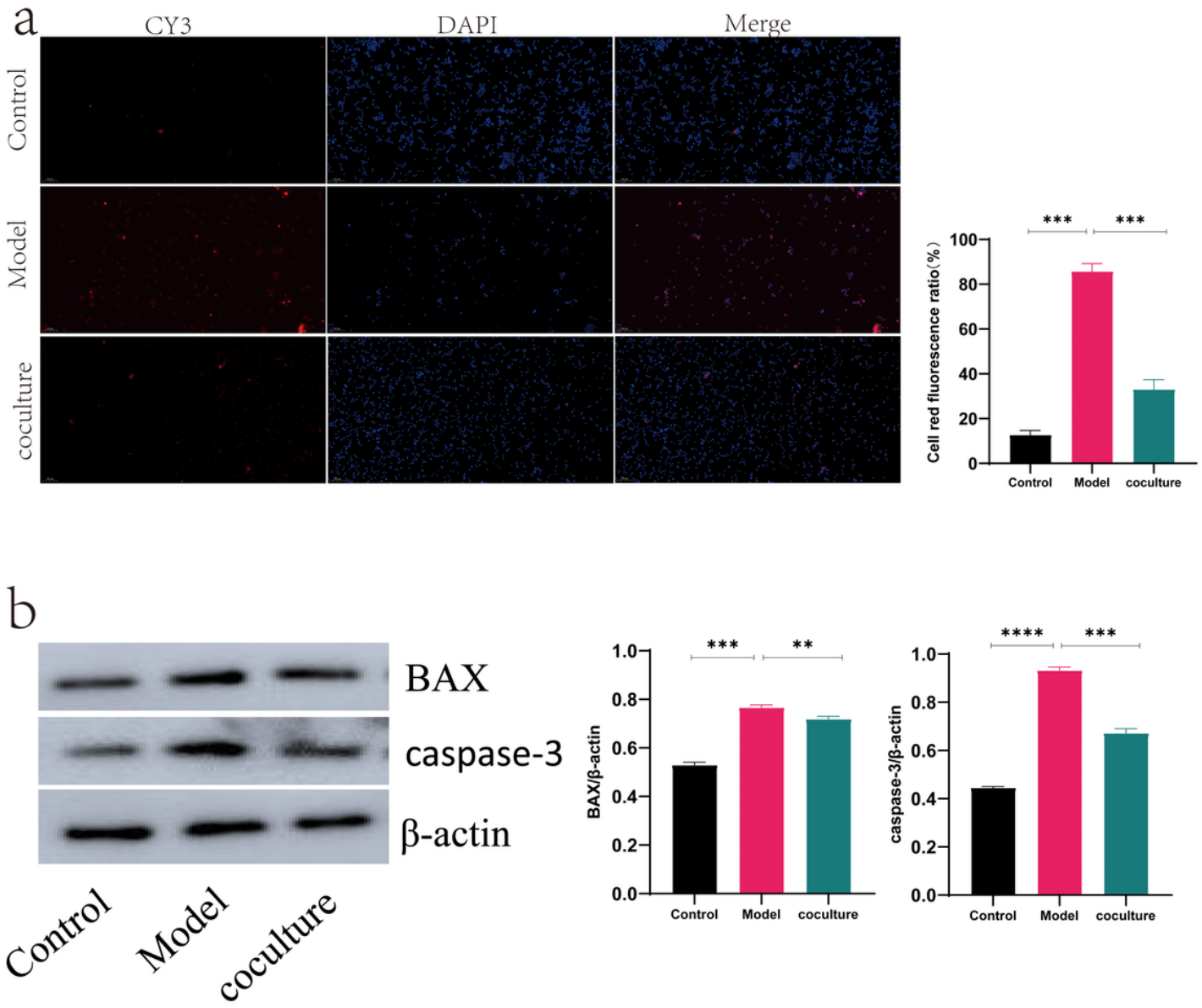

Figure 2

Protective effect of UCMSCs against H_2O_2-induced TEC apoptosis. (a) The effect of UCMSCs on H_2O_2-induced apoptosis was detected by TUNEL staining (n = 3, n is the number of cells analyzed; ***P< 0.001 vs. the control group, ***P<0.001 vs. the model group). (b) western blot analysis of the apoptosis-related proteins Bax and caspase-3 (n = 3, n is the number of cells analyzed; ****P<0.0001, ***P<0.001, ** P<0.01).

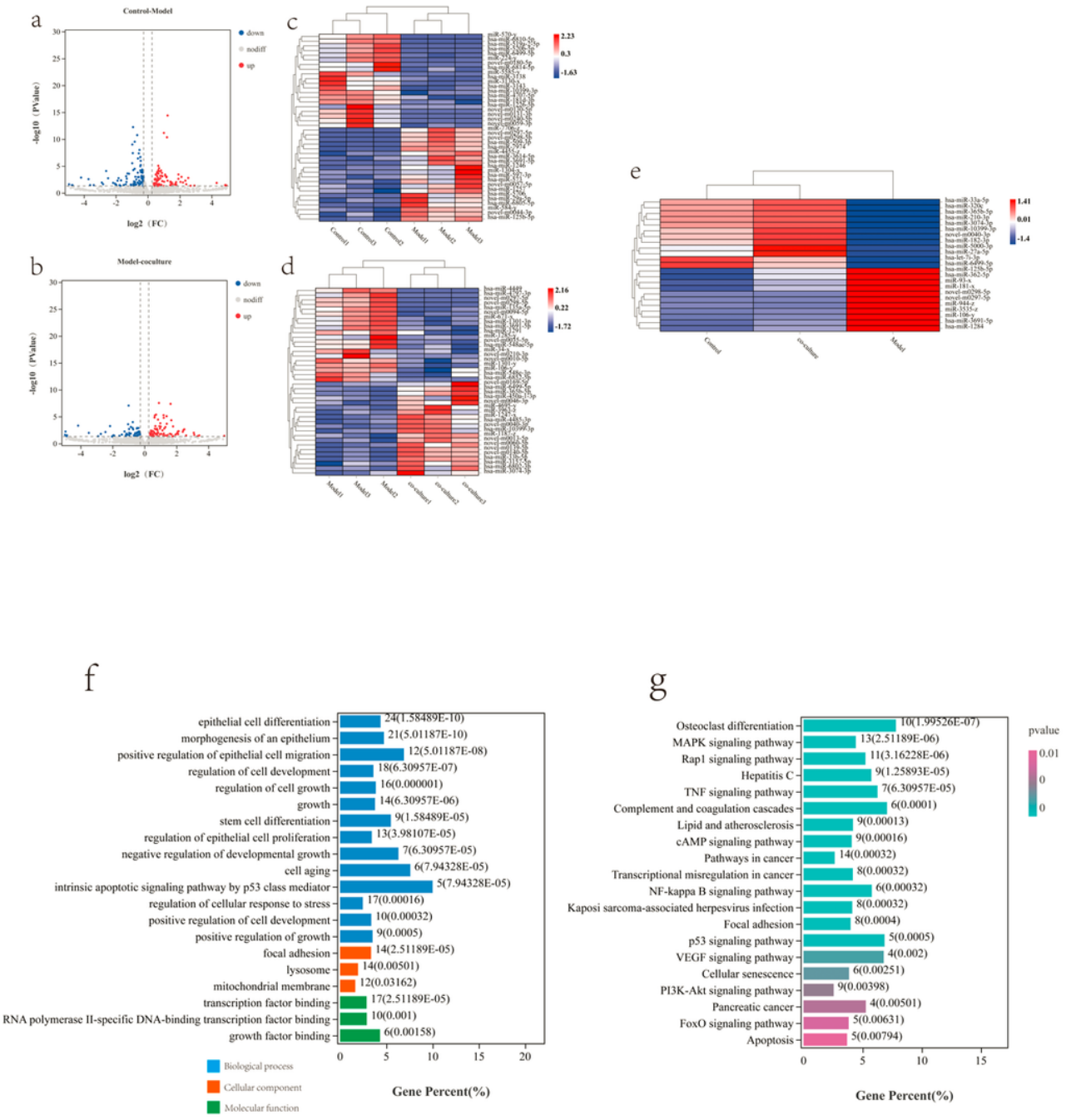

Figure 3

Differential expression analysis of mRNAs. (a) Volcano plot of the differential mRNA expression profiles of the control group and model group. (b) Volcano plot of the differential mRNA expression profiles of the model group and coculture group. Unsupervised cluster analysis showed (c) the expression profiles of the top 20 up- and downregulated mRNAs between the control and model groups and (d) the expression profiles of the model and coculture groups. (e) Heatmap showing that 272 mRNAs showed altered expression when TECs were treated with H_2O_2; treatment with UCMSCs reversed these changes.

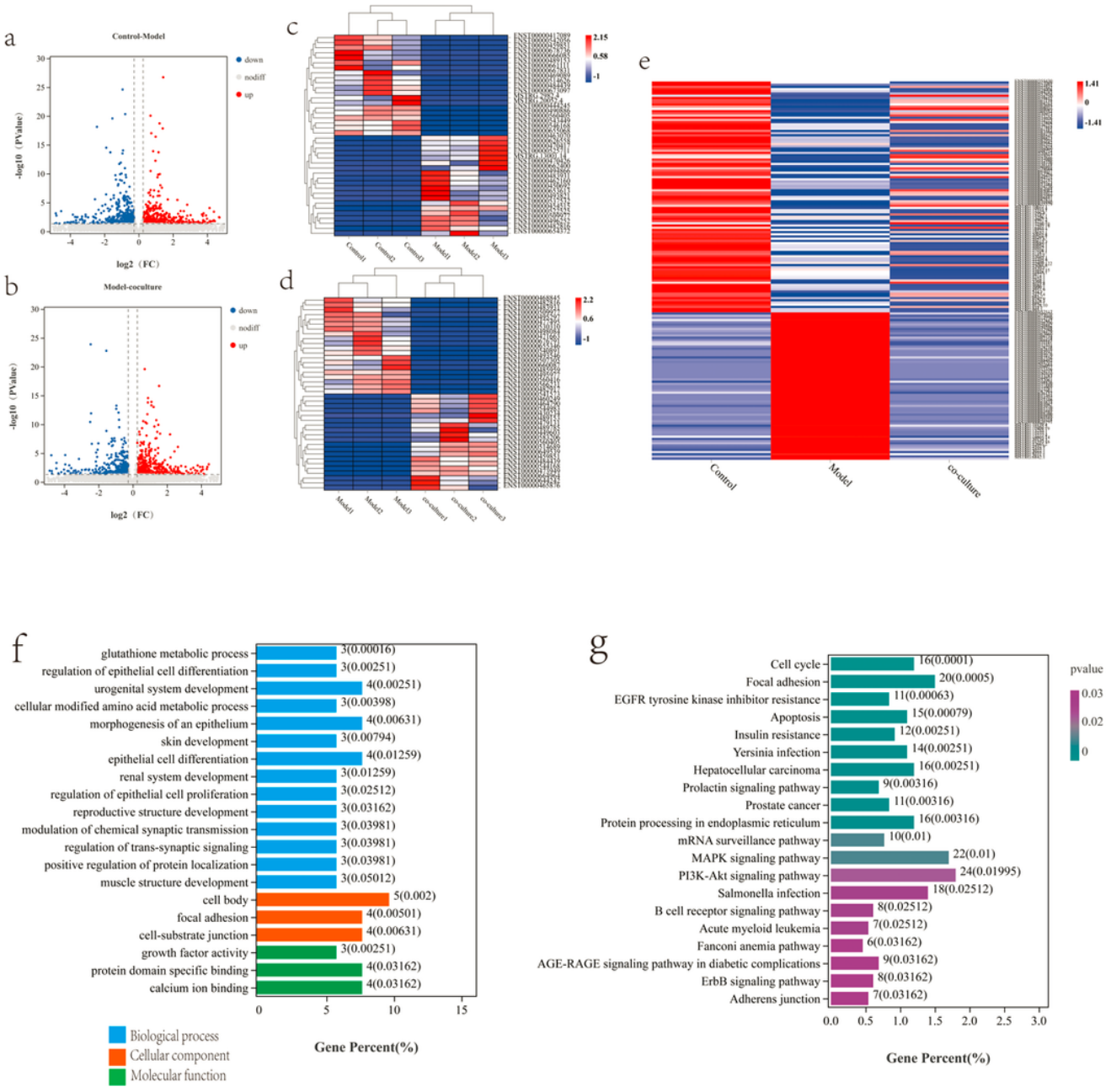

Figure 4

Analysis of differential expression of lncRNAs and volcano plots of the expression profiles of differentially expressed lncRNAs (a) between the control group and the model group and (b) between the model group and the UCMSC group. Unsupervised cluster analysis showed the expression profiles of the top 20 up- and downregulated lncRNAs (c) between the control and model groups and (d) between the model and coculture groups. (g) Heatmap showing 172 lncRNAs that were altered by H2O2 in TECs; treatment with UCMSCs reversed these alterations. As shown in Figure (4e),

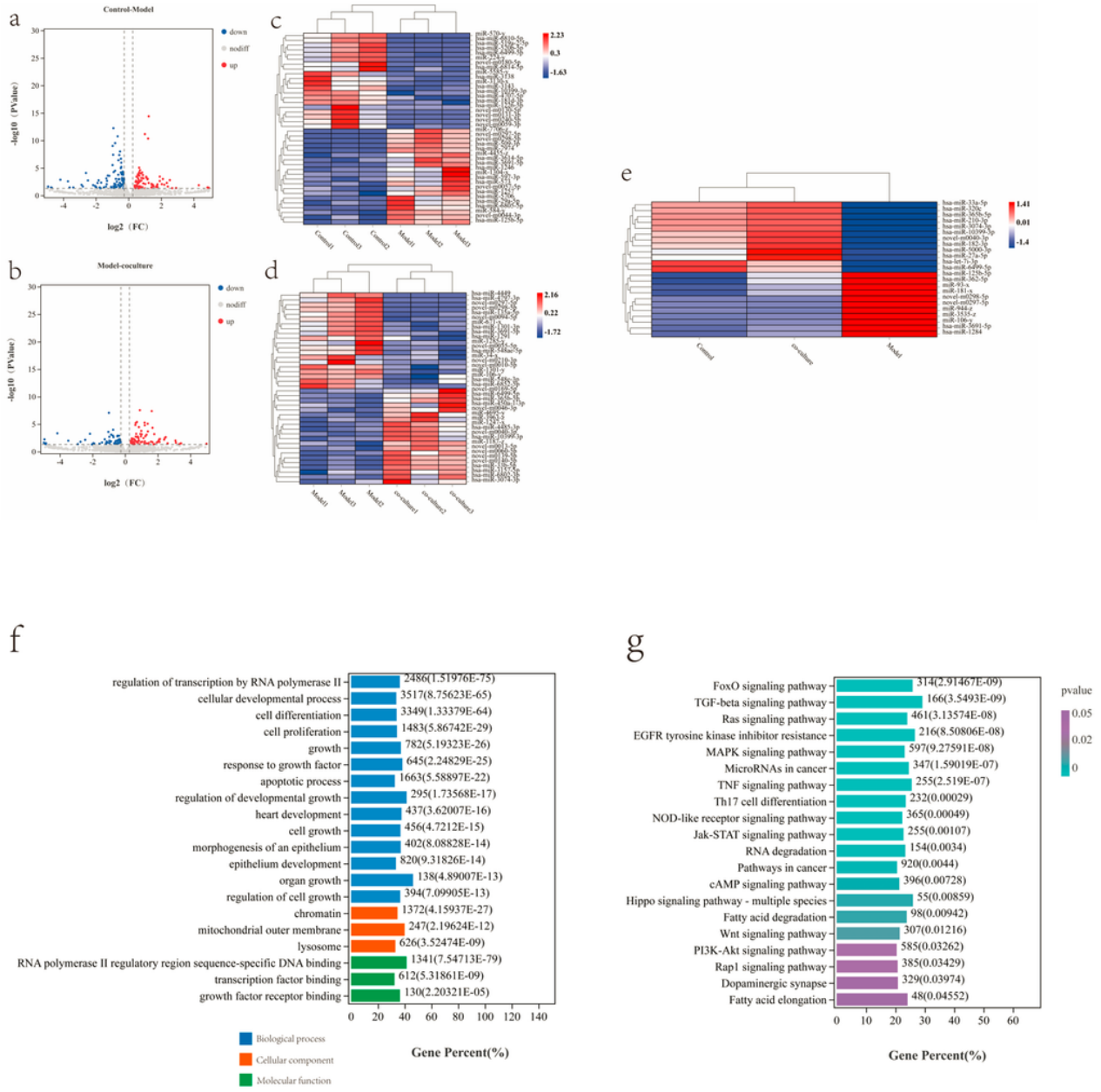

Figure 5

Differential expression analysis of miRNAs and volcano plots of DE miRNA expression profiles (a) between the control and model groups and (b) between the model and coculture groups. Unsupervised cluster analysis showed the expression profiles of the top 20 miRNAs that were up- and downregulated between the control and model groups. (c) and (d) The expression profiles of the model and coculture groups. (e) Heatmap showing 23 miRNAs that were altered when TECs were subjected to H_2O_2-induced senescence, which was reversed by UCMSCs.

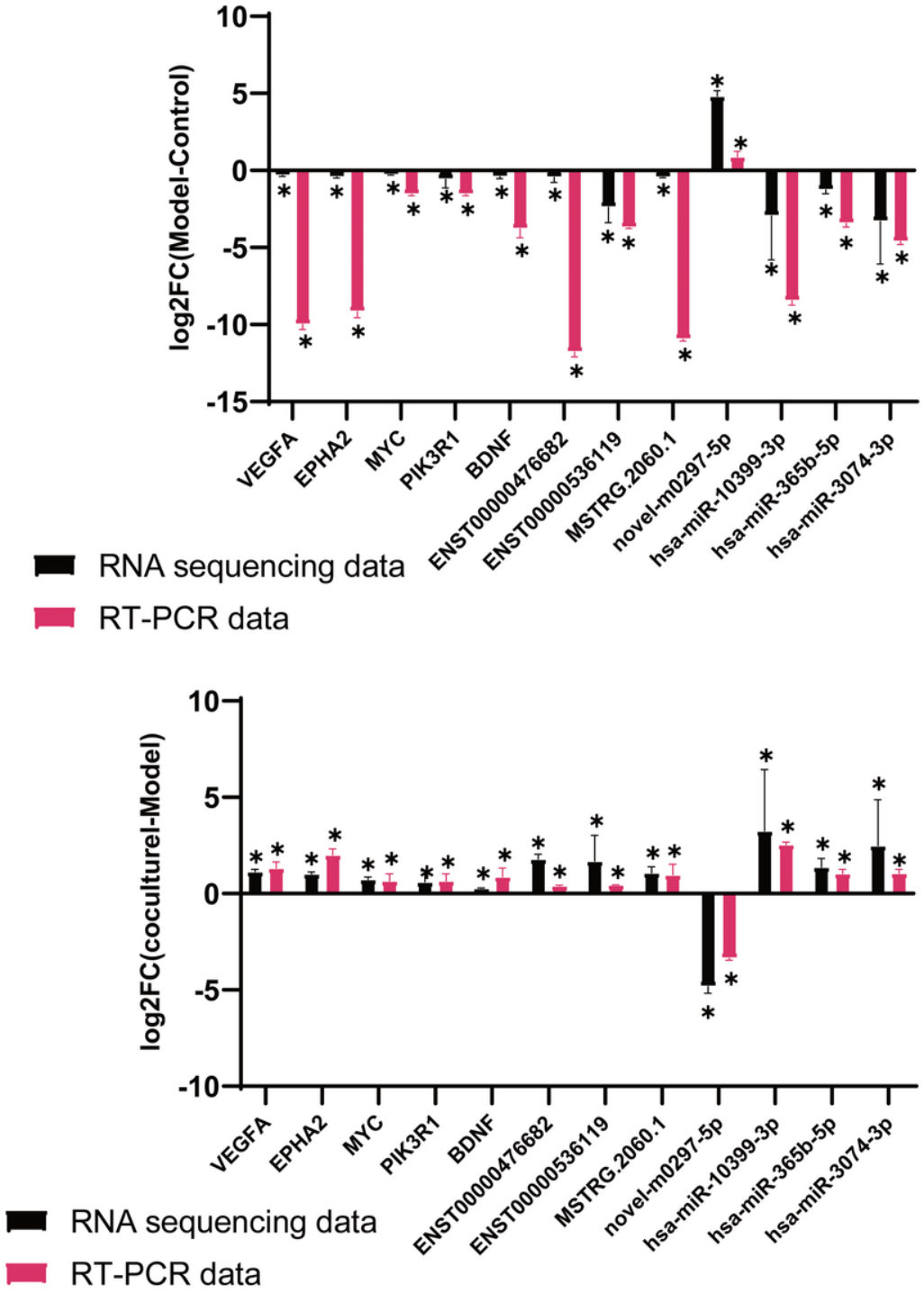

Figure 6

RT–qPCR-validated differential expression of ncRNAs and mRNAs. The data show that the expression levels of lncRNAs (ENST00000476682, ENST00000536119, MSTRG.2060.1), microRNAs (novel-m0297-5p, hsa-miR-10399-3p, hsa-miR-365b-5p, hsa-miR-3074-3p, hsa- miR-3691-5p), and mRNAs (VEGFA, EPHA2, BDNF, MYC, PIK3R1) and the RT–qPCR results were consistent with the RNA sequencing results.

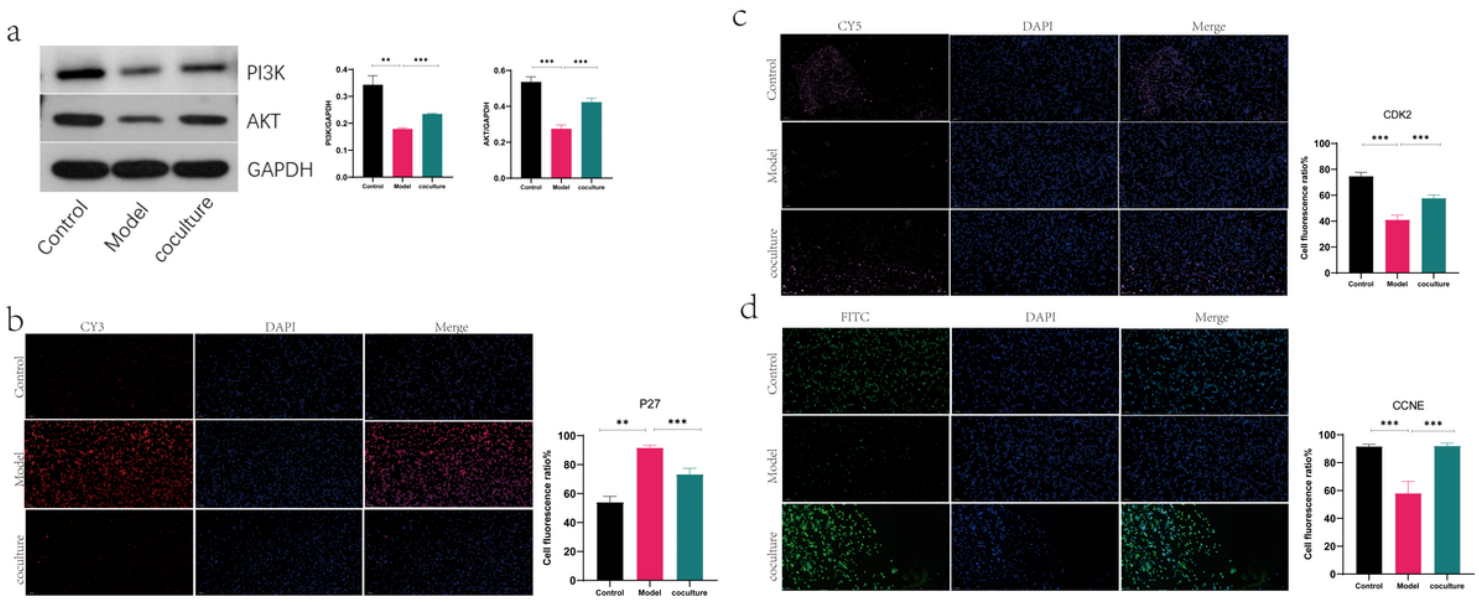

Figure 7

UCMSCs activate the PI3K-AKT pathway in senescent TECs. (a) The expression of PI3K-AKT signaling pathway proteins was detected by western blotting, and GAPDH was used as a control. (b-d) Immunofluorescence detection of the expression of p27, CDK2 and CCNE at key sites of cell cycle regulation downstream of the PI3K signaling pathway.

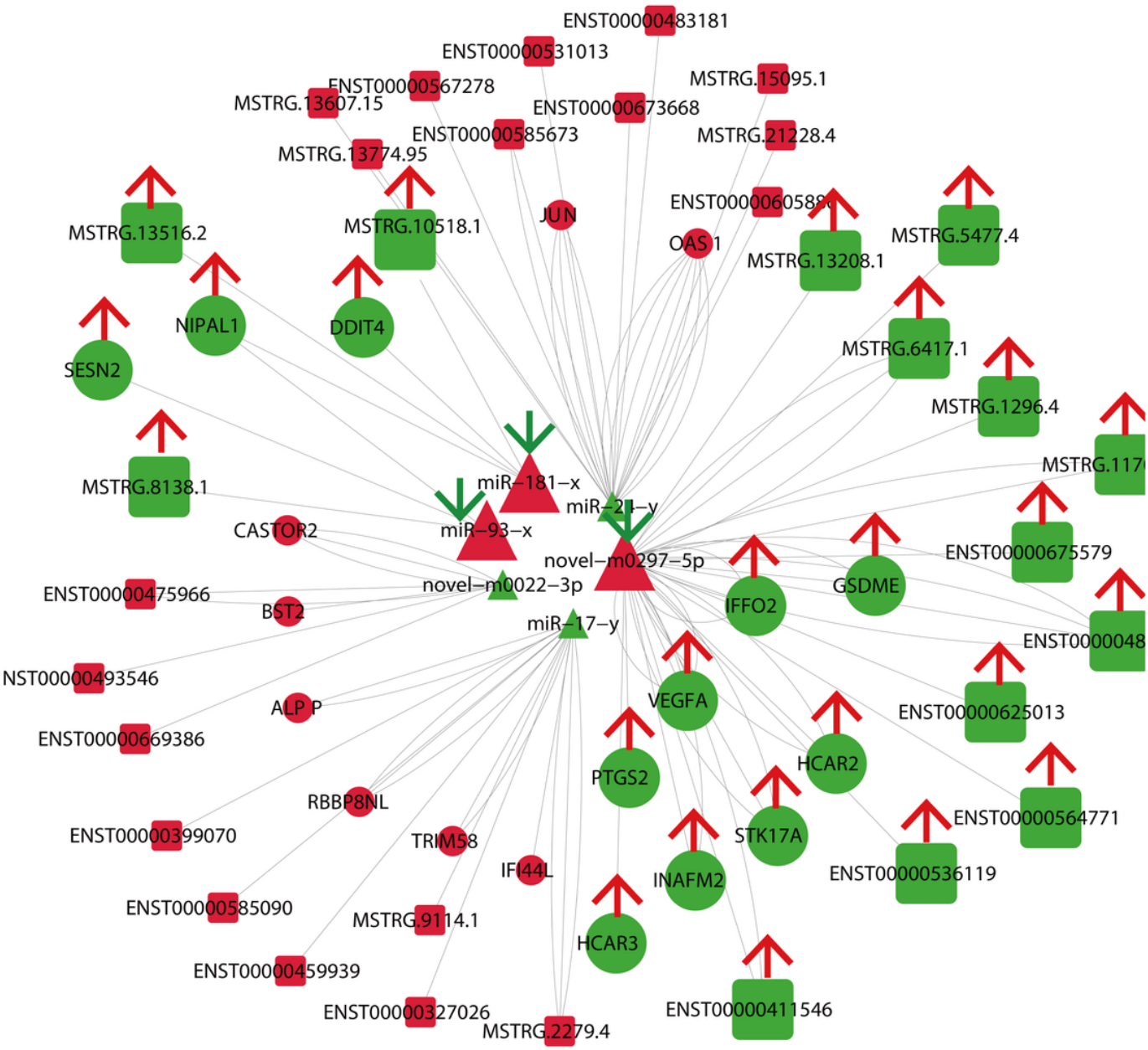

Figure 8

LncRNA-miRNA–mRNA interaction network. Circles represent mRNAs, squares represent lncRNAs, and triangles represent miRNAs. Red and green represent up- and downregulation in the model group, respectively. Arrows indicate UCMSC-altered RNAs, and downward arrows indicate downregulation.